INGV-T3 Research Project 2015-2016

HYPSTHER

HYBRID GROUND MOTION PREDICTION EQUATIONS FOR PSHA PURPOSES: THE STUDY CASE OF SOUTHERN ITALY

Task 3 (WG-T3)

GMPEs calibration

Giovanni Lanzano[(1)], Maria D'Amico[(1)], Chiara Felicetta[(1)] and Rodolfo Puglia[(1)]

[(1)] Istituto Nazionale di Geofisica e Vulcanologia: Sezione di Milano, Via Corti 12, 20133 Milano, Italy

Abstract

The WG-T3 will develop a set of Ground Motion Prediction Equations (GMPEs) for Italy or significant regions, using the results of the previous tasks. In particular, two subsets of GMPEs will be retrieved:

- Empirical GMPEs based on the flat-file of recorded waveforms developed in Task 1;
- Hybrid GMPEs based on the flat-file integrating the recorded and simulated data;

The results will be compared among them and with respect to other significant existing GMPEs. The goodness of fit will be evaluated on the basis of the residuals, calculated as the difference between observations and predictions.

The standard deviation (σ) of the total residuals of GMPEs has a strong influence on the results of PSHA. In most GMPEs, the aleatory variability is assumed to be homoscedastic, i.e., independent of the variables included in the equation. Several authors have found trends relating the sigma to one or more explanatory variables and therefore suggested heteroscedastic models, in which σ depends on the predictor variables. In this document, we propose a heteroscedastic model for the hybrid GMPEs, including a dependence on magnitude. These values will be compared to those evaluated for other world regions. This variability model will be adopted to perform region-specific Probabilistic Seismic Hazard Assessment (PSHA) in Southern Italy.

Keywords: *GMPEs; median prediction; standard deviation; heteroscedastic model; hybrid-GMPEs*

Introduction

In the last decades, the calibration of reliable GMPEs in a region of interest became a critical issue in PSHA. GMPEs generally describe the amplitude of the ground shaking as function of magnitude distance and site condition and they are generally derived from empirical data of past events, when available.
The most known and used GMPEs were derived from strong motion data of worldwide areas where dense recording networks are present, such as California, Japan, Turkey and Italy. In the framework of the NGA (New Generation Attenuation) research project, five empirical GMPEs were developed in order to provide ground motion characterization (GMC) models for Western US, collected thousands of data from few well-monitored countries (Bozorgnia et al. 2014). In Europe, several GMPEs were calibrated on the basis of strong-motion database of European and Middle-Eastern waveforms (RESORCE, Akkar et al. 2014a) in the framework of the SeIsmic Ground Motion Assessment (SIGMA; project- sigma.com) project (Douglas et al. 2014).
In areas characterized by high hazard levels where few significant earthquakes occurred in the recent years or the recording network is not sufficient, the empirical data can be scarce and the use of synthetic ground motion parameters is a possible way to represent the ground motion in the region of interest. Indeed, when the site is very close to the fault, the rupture processes are predominant and the finite-source effects, such as directivity, hanging wall/foot wall, radiation-pattern and slip distribution dominate the GMCs. Therefore, the empirical GMPEs are generally incapable to captures such features, because the strong motion records in near source are few.
In the recent years, some research projects included the use of synthetic data to fill the lack of observations, especially for moderate to large earthquakes in near field conditions. In particular, NGA-East project (Goulet et al. 2011) provides a set of new GMPEs for median and standard deviation of Ground Motions (GMs) for use in PSHA for Central and Eastern North-American Region, on the basis of synthetic data: the median predictions are developed incorporating point-source and finite-fault simulations, while standard deviations are modelled only on empirical basis. Some efforts were also done in the calibration of physics-based GMPEs, which are particularly effective in showing important ground motion features in near source regions (NERA EU Project, Dalguer et al. 2014).
A common approach to obtain and hybrid description of the ground motion in a given area is the *host-to-target* method (Campbell, 2003), which calibrates an empirically well-constrained GMPE in a data-rich host region for use in a data-poor target region based on adjustment factors obtained from response-spectral ratios of stochastic simulations in the host and target regions. Another method is the empirical approach introduced by Atkinson (2008), for which the adjustment factors are determined using spectral ratios of observed motions in the target region to predictions of an empirical GMPE in the host region. Yenier and Atkinson (2015) used this method to develop a GMPE for North-Eastern US by adjusting the stress and anelastic attenuation, and calibrate the model using the NGA-East database.
This deliverable presents the findings of the Task 3 of the project *HYPSTHER* (HYbrid ground motion prediction equations for PSha purposes: the study case of souTHERn Italy). The goal of the Task 3 is to develop a methodological approach to retrieve ground motion prediction models, based on the integration between recorded and synthetic data. The main contents of the document are:

- Description of the empirical dataset to be used to characterize the ground motion in the shallow active crustal regions of Southern Italy (Southern Calabria and Sicily), on the basis of the outcomes of the Task 1 (Puglia et al. 2018);
- Ranking of the existing GMPEs on the basis of the empirical dataset, using the LLH (Scherbaum et al. 2009) as a metric for the scoring procedure;
- Calibration of empirical GMPEs, including the reference rock sites, recognized by Task 1;
- Calibration of hybrid GMPEs for outcropping rock, merging the empirical dataset and those provided by Task 2 (D'Amico et al. 2018) on the basis of the synthetic databases: EXSIM (Generic Source, GS_DTS) and SMSIM (Pulse-Like Source, PLS_DTB);
- Development of a heteroscedastic model for aleatory variability of the hybrid GMPEs.

Dataset

The work of the project Task 1 (Puglia et al. 2018) resulted in collecting about 3200 three-component waveforms for the study area, according to the following criteria:

- latitude: min = 34, max = 40; longitude: min = 10, max = 18 (spatial limits valid for both stations and events);
- $M_W \geq 3.5$ (or, in case of missing value for MW, ML ≥ 3.5);
- epicentral distance, $R_{epi} \leq 200$ km;
- recordings of strong-motion (acceloremetric) and broad-band (velocimetric) instruments.

For GMPEs calibration and testing, we exclude the deep subduction (inslab) events of the Calabrian Arc and the volcanic events of Mount Etna and Aeolian Islands, with depth lower than 5km, since the ground-motion is significantly different from the shallow active one (Tusa and Langer, 2017; Michelini et al. 2017).

In the dataset, several recording stations have co-located instruments (accelerometer and broad-band), which frequently recorded the same events. When we have two records for the same station and the same event, we decided to include in the calibration dataset only the broad-band waveform, if not saturated, in order to avoid oversampling. The main reason is related to the better quality of broad-band recordings (low noise level), compared to those obtained from accelerometric instruments.

The empirical dataset for shallow active crustal earthquakes included 1942 records of 133 events. Figure 1a reports magnitude – distance distribution, still highlighting the scarcity of recorded data for magnitudes larger than 4.7 and in near fault conditions. Figure 1b shows the histogram of data with respect to focal mechanisms: the reverse faulting (TF) events are not well represented in the dataset; the majority of data is related to undefined style of faulting (about 44%).

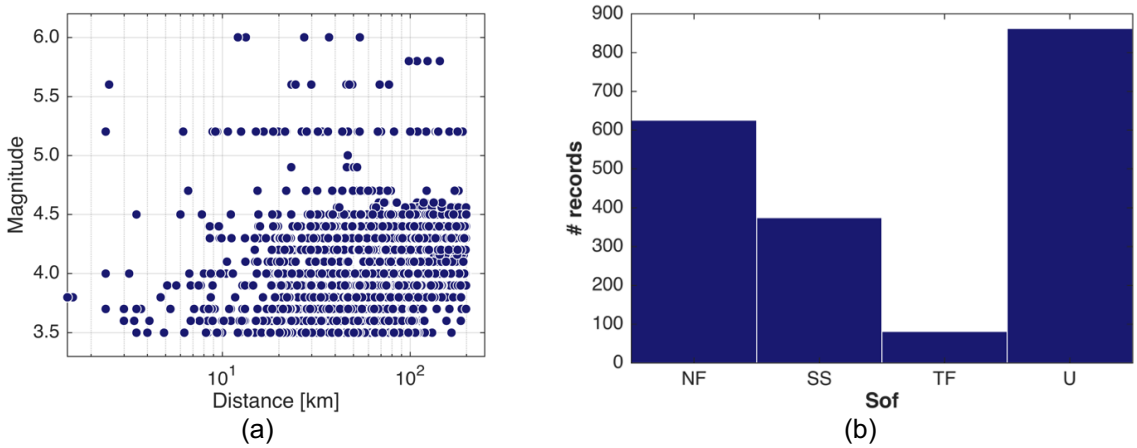

Figure 1. *Dataset for the calibration of the empirical GMPEs: a) Magnitude – distance distribution; b) distribution of the records as a function of focal mechanism (NF: normal; SS: strike-slip; TF: reverse; U: undefined).*

Figure 2 shows the maps of the events with respect to magnitude, event depth and style of faulting. The dataset encompasses a significant number of events in the Eastern Sicily, especially in Etna and Aeolian islands; a consistent amount of data in Calabria is related to the recent 2012 Pollino seismic sequence (mainshock M_W 5.2).

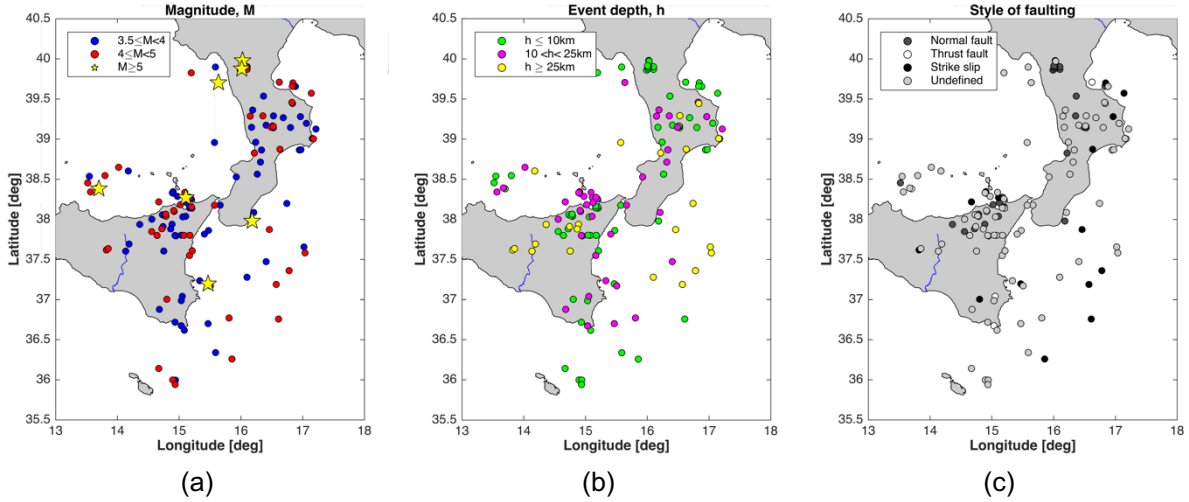

Figure 2. *Maps of the events included in the empirical dataset of shallow active crustal regions. The circles are colored as a function of: a) magnitude; b) focal depth; c) style of faulting.*

Figure 3a shows the spatial distribution of the 194 recording stations of the dataset as a function of the EC8 site classification (CEN, 2004). Figure 3b reports the location of the reference rock sites, recognized by Puglia et al. (2018): they are mainly located in Calabria and in the Northern Sicily.

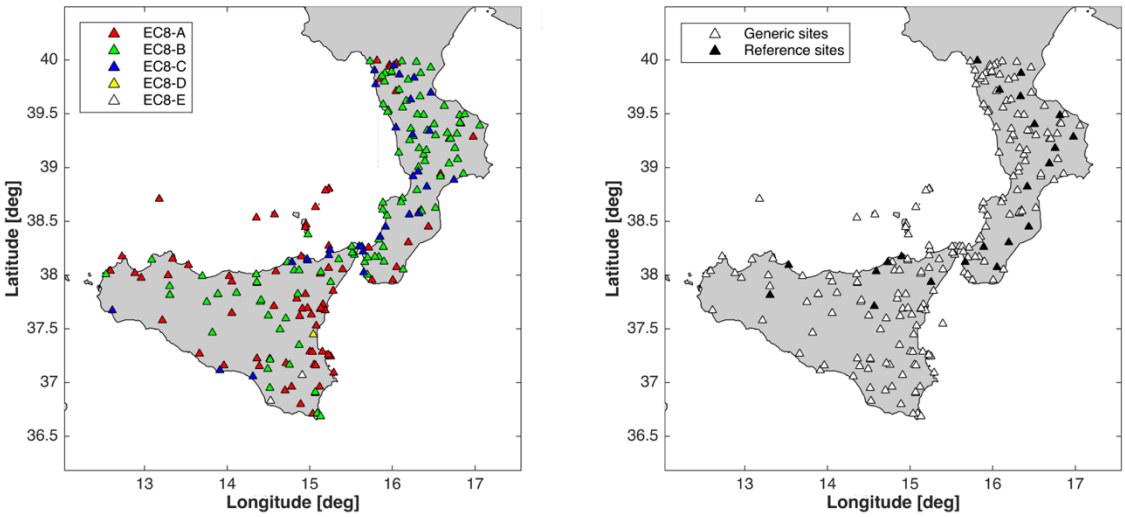

(a) (b)

Figure 3. *Map of recording stations of the empirical dataset. The triangles are colored as a function of: a) EC8 site category; b) reference rock and generic site according to Puglia el al. (2018).*

Ranking of GMPEs

In this section, the performance of the existing GMPEs against the empirical data collected in Southern Italy is evaluated. We select a set of GMPEs, which are valid for active shallow crustal regions and not rejected by the criteria of Cotton et al. (2006) and Bommer et al. (2010), with the exception of Akkar & Bommer (2010), which is superseded by Akkar et al. (2014b): we decided to include this model because it was used for PSHA in Europe (e.g. in the framework of SHARE EU project, Woessner et al. 2015).

In Table 1, the characteristics of the selected GMPEs are given in terms of magnitude ranges, distance type, site classes and style of faulting: the suite of GMPEs encompasses 3 prediction models for Europe, 5 worldwide models and only one for Italy. The European models include mainly strong-motion data from Mediterranean and the Middle East regions (Italy, Greece, Turkey and Iran); four global models are calibrated in the framework of the NGA-West2 project, on the basis of the same dataset (Ancheta et al. 2014); the model by Cauzzi et al. (2015) is mainly derived from Kik-Net Japanese data; the model by Bindi et al. (2011) can be considered the reference GMPEs for Italy and included waveforms of Italian events from 1976 to 2009, with a small contribution of events occurred in Calabria and Sicily.

Although most of the models consider events with magnitude up to 7.9 and distances down to 0 km, the near-source observations for strong events are generally sparse, with the exception of model by Campbell and Bozorgnia (2014), calibrated with several records (about 7200) of moderate and large magnitude events, within 80 km from the source.

Table 1. *List of the candidate GMPEs for ranking analysis.*

Name	Code	Area	Magnitude range	Distance type	Site class	Style of faulting
Bindi et al (2011)	ITA10	Italy	4.1 - 6.9	R_{JB}	EC8	N, R, SS, U
Akkar and Bommer (2010)	AB10	Europe	5.0 - 7.6	R_{JB}	EC8	N, R, SS
Abrahamson et al (2014)	ASK14	Worldwide	3.0 - 7.9	R_{rup}	$V_{S,30}$	N, R, SS, HW
Boore et al (2014)	BSSA14	Worldwide	3.0 - 7.9	R_{JB}	$V_{S,30}$	N, R, SS, U
Campbell & Bozorgnia (2014)	CB14	Worldwide	3.0 - 7.9	R_{rup}	$V_{S,30}$	N, R, SS, HW
Chiou & Youngs (2014)	CY14	Worldwide	3.1 - 7.9	R_{rup}	$V_{S,30}$	N, R, SS, HW
Akkar et al (2014)	ASB14	Europe	4.7 - 7.6	R_{JB}	$V_{S,30}$	SS, R, N
Akkar et al (2014)	ASB14	Europe	4.7 - 7.6	R_{hypo}	$V_{S,30}$	SS, R, N
Bindi et al (2014)	BND14	Europe	4.0 - 7.6	R_{JB}	EC8	SS, R, N, U
Bindi et al (2014)	BND14	Europe	4.0 - 7.6	R_{hypo}	EC8	SS, R, N, U
Cauzzi et al (2015)	CZ15	Worldwide	4.5 - 7.9	R_{rup}	$V_{S,30}$	SS, N, R

Distance type: *R_{JB} = Joyner-Boore distance; R_{hypo} = hypocentral distance; R_{rup} = rupture distance.*
Style of faulting: *N = Normal faulting; R = Reverse faulting; SS = Strike-slip faulting; U = not available; HW = Hanging wall effect.*

Most of the ranking schemes are based on the calculation of the residuals, i.e. the logarithmic difference between observations and predictions, normalized with respect to the model standard deviation. The basic assumption on residuals is that they are normally distributed.
In this work, we adopted the well-known ranking procedure proposed by Scherbaum et al (2009), which measure the performance through the Log-LikeliHood (LLH). The method is based on the information theory and evaluates the probability for an observed ground motion model to be realized under the hypothesis that an empirical model is true (Delavaud et al., 2009). LLH measures the distance between a model and the data-generating distribution (i.e. distribution of the normalized residuals) as:

$$LLH(g,x) = -\frac{1}{N}\sum_{i=1}^{N}\log_2(g(x_i)) \qquad [1]$$

where N is the number of observations x_i and $g(x_i)$ is the probability density function (PDF) that model g has produced the observation x_i. Small absolute values of LLH indicates that the candidate GMPEs are close to the model that has generated the data.
If x_i has been used for the derivation of the model (e.g. for calibration of the coefficients), the log-likelihood will underestimate the true information loss and the model will appear better than it really is by an amount that depends on the degree of freedom of the model. In this case, this problem slightly affects the results, since a very small amount of empirical data used in this analysis (less than 10 %), was employed for the derivation of the selected GMPEs.
Very few records are provided of moment magnitude values (Puglia et al. 2018): hence, notwithstanding that the majority of the employed GMPEs are calibrated over Mw, in our analysis we perform residuals and LLH ranking employing ML when moment magnitude is not available. Since several GMPEs include in the functional form a dependency on $V_{S,30}$ to

describe the site effects, the average shear wave velocities were estimated using empirical correlation to link the topographic slope to $V_{S,30}$, as proposed by Wald and Allen (2007), for recording sites missing of *in-situ* measurement.
The LLH results are given in Table 2 for five intensity measures (IMs), commonly employed for shakemaps evaluation (PGA, PGV and three ordinates of the 5% acceleration response spectra). We have determined the final ranking on the mean values of LLH, calculated over the investigated parameters.

Table 2. *LLH of the candidate GMPEs.*

LLH	PGA	SA(0.3s)	SA(1s)	SA(3s)	PGV	mean
ITA10	2.518	2.260	1.948	1.938	2.079	*2.149*
ASB14 Rjb	3.839	2.410	1.868	1.848	2.433	*2.480*
AB10	6.557	3.833	2.117	2.001	3.068	*3.515*
BSSA14	2.470	2.255	2.202	2.003	2.013	*2.189*
BND14 Rjb	3.274	2.388	1.946	1.953	2.051	*2.322*
ASB14 Rhypo	3.295	2.218	1.819	1.842	2.188	*2.272*
CZ15	4.840	2.555	1.900	1.807	3.523	*2.925*
BND14 Rhypo	2.856	2.305	1.937	1.928	1.900	*2.185*
ASK14	2.735	2.218	1.993	1.963	2.132	*2.208*
CY14	2.805	2.205	1.997	2.086	2.055	*2.230*
CB14	2.519	2.201	2.218	2.321	2.042	*2.260*

We found that the best performing models are the model by Bindi et al. (2011) for Italy (#1), the European one by Bindi et al (2014) in hypocentral distance (#2) and the global GMPEs by Boore et al. (2014) (#3). The first and the second are characterized by almost the same functional form, while the model BSSA14, like most of the NGA-West2 models, are characterized by a more complex mathematical expression of the GMPEs. The worst performing model is that provided by Akkar and Bommer (2010), because it was calibrated with recording data within 100km and magnitudes larger than 5.0, not well represented by our testing dataset.
With the aim of identifying the reason why GMPEs are appropriate or not to explain the data, Figure 4 represents the total residuals of three models (ITA10, CZ15 and AB10) as a function of distance for two IMs (PGA and spectral acceleration ordinate at T=3s).

ITA10 exhibits larger variability at shorter periods, as observed for the majority of the GMPEs. The residuals trend with distance is only slightly biased, with negative values at shorter period for distances R<50km and longer periods for R>100km. CZ15 shows an inadequate performance for PGA, especially in the distance range where the dataset is well sampled (50-150km). On the contrary, it has the best performance at longer periods, since it was calibrated with a large number of good-quality digital records. AB10 displays strongly negative PGA residuals at all distances.

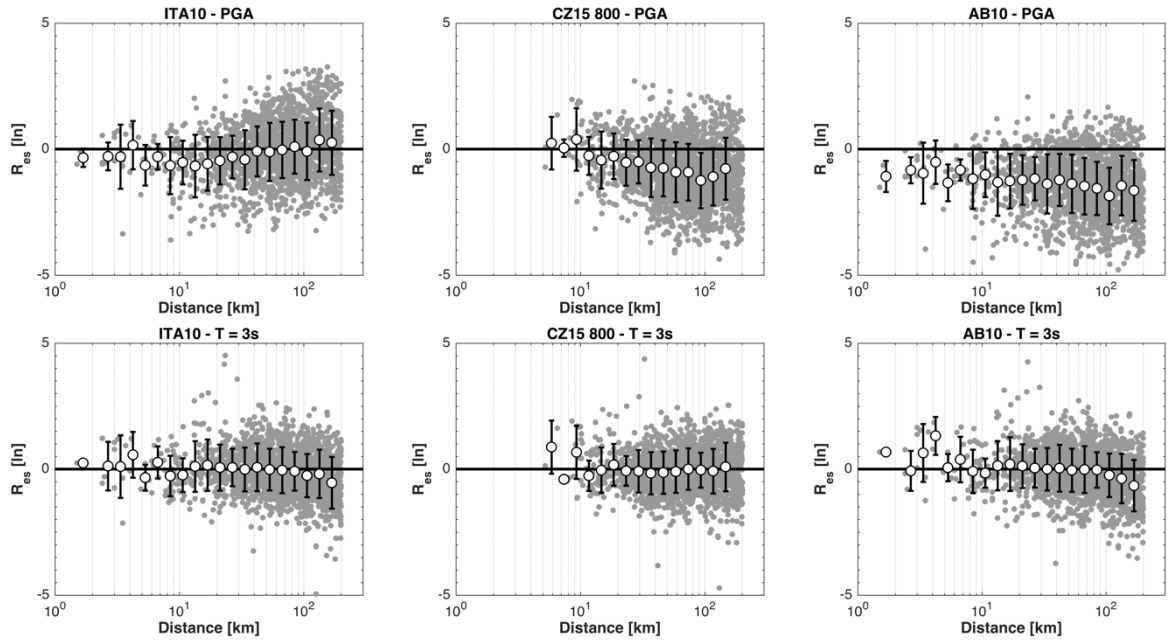

Figure 4. *Residuals trend with distance of ITA10, CZ15 and AB10 (see Table 1) for PGA and spectral acceleration at T=3s.*

Empirical GMPEs

We select a subset of events with magnitude larger than 4.0 and focal depth lower than 25km. Few records with large residuals, calculated with respect to the best performing GMPEs of Table 2 (i.e. Bindi et al. 2011), have been also excluded (they are listed in the Appendix I). The calibration dataset included 840 records of 48 events recorded by 194 stations. We adopt the functional form of the ITA10, with some modifications:

$$log_{10}Y = a + F_D(R,M) + F_M(M) + F_S + F_{sof} \quad [2]$$

where a is the offset; F_D is the distance term:

$$F_D(R,M) = \left[c_1 + c_2\left(M - M_{ref}\right)\right] log_{10}\left(\frac{\sqrt{R^2+h^2}}{R_{ref}}\right) \quad [3]$$

where M is the moment magnitude (or the local magnitude without conversion, if the moment magnitude is not available), R is the Joyner-Boore distance (or the epicentral distance when the fault geometry is not known). The reference magnitude (M_{ref}=5.0) and distance (R_{ref}=1km) were assumed equal to ITA10. The pseudo-depth h and the coefficients c_1 and c_2 were derived from data regression. Differently from ITA10, the anelastic attenuation in the distance term has been neglected.

F_M is the magnitude term:

$$F_M(M) = \begin{cases} b_1(M - M_h) + b_2(M - M_h)^2 & for\ M \le M_h \\ 0 & otherwise \end{cases} \quad [4]$$

where M_h is the hinge magnitude, assumed equal to 6.75 as in ITA10; b_1 and b_2 are the calibration coefficients.
$F_{sof} = f_j E_j$ (with j = NF, SS and U) is the style of faulting term, where E_j are dummy variables and f_j are the regression coefficients. We set the coefficients of class U to 0 and neglected the reverse fault records (TF) because they are not well represented in the dataset (see Figure 1b). $Fs = s_i S_i$ (with i = RR, GR, ST and SO) is the term which describes the site effects: S_i are dummy variables and s_i are the coefficients for 4 soil classes: i) reference rock (RR), i.e. the stations in Puglia et al. (2018); ii) generic rock (GR), i.e. sites of A class, according to EC8 (CEN, 2003), which cannot be considered ad a reference rock sites (affected by amplification, etc.); iii) stiff soil (ST), i.e. sites of EC8-B and EC8-E classes; iv) soft soil (SO), i.e. sites of EC8-C and EC8-D classes. In the regression, the coefficient of class RR is set to 0. Figure 5 shows the distribution of the records for each site class in the dataset: the percentages are 19.4% for RR, 36.4% for GR, 33.5% for ST and 10.7% for SO.

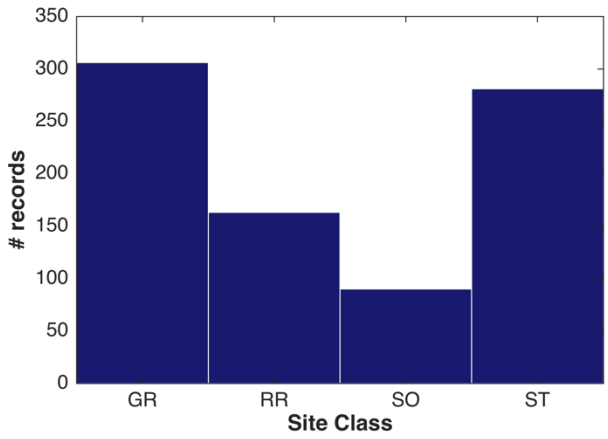

Figure 5. *Histograms of the number of records for each soil classes of the GMPEs. GR: generic rock; RR: reference rock; SO: soft soil; ST: stiff soil.*

The GMPEs were calibrated for the geometric mean of horizontal components of PGA, PGV and 3 ordinates of the 5% damping acceleration response spectra (0.3, 1 and 3s), that are commonly used for the shakemaps calculation (Wald et al. 2006). Since the spectral ordinates included in the regression are consistent with the waveform-filtering interval, only 832 records are used for the GMPE calibration at T = 3s.
The regressions are performed by applying the random effect approach (Abrahamson and Youngs, 1992), separating the total residual into between-event and within-event terms (Al-Atik et al. 2010). The calibration coefficients of the empirical GMPEs (named SI17ref) are given in Table 3, where σ, τ and ϕ are the standard deviations of the total, between-event and within-event residuals, respectively.

Table 3. *Coefficients of SI17ref.*

IM	a	b_1	b_2	c_1	c_2	h [Km]	f_{NF}	f_{SS}	s_{GR}	s_{ST}	s_{SO}	τ	ϕ	σ
PGA	3.863	0.004	-0.070	-2.039	0.222	11.91	0.036	-0.036	0.479	0.475	0.617	0.107	0.322	0.339
SA 0.3s	4.526	0.375	-0.041	-1.884	0.099	12.24	0.037	-0.037	0.488	0.448	0.607	0.112	0.335	0.353
SA 1s	3.929	0.467	-0.122	-1.548	-0.010	11.16	0.018	-0.018	0.370	0.295	0.484	0.107	0.320	0.337
SA 3s	2.383	0.369	-0.083	-1.301	0.241	10.54	0.058	-0.058	0.335	0.228	0.416	0.135	0.320	0.348
PGV	2.568	0.279	-0.041	-1.712	0.228	11.46	0.027	-0.027	0.413	0.381	0.569	0.098	0.295	0.311

In Figure 6, the total and between-event residuals of SI17ref are plotted for PGA and PGV: the trends with distance and magnitude were found to be unbiased.

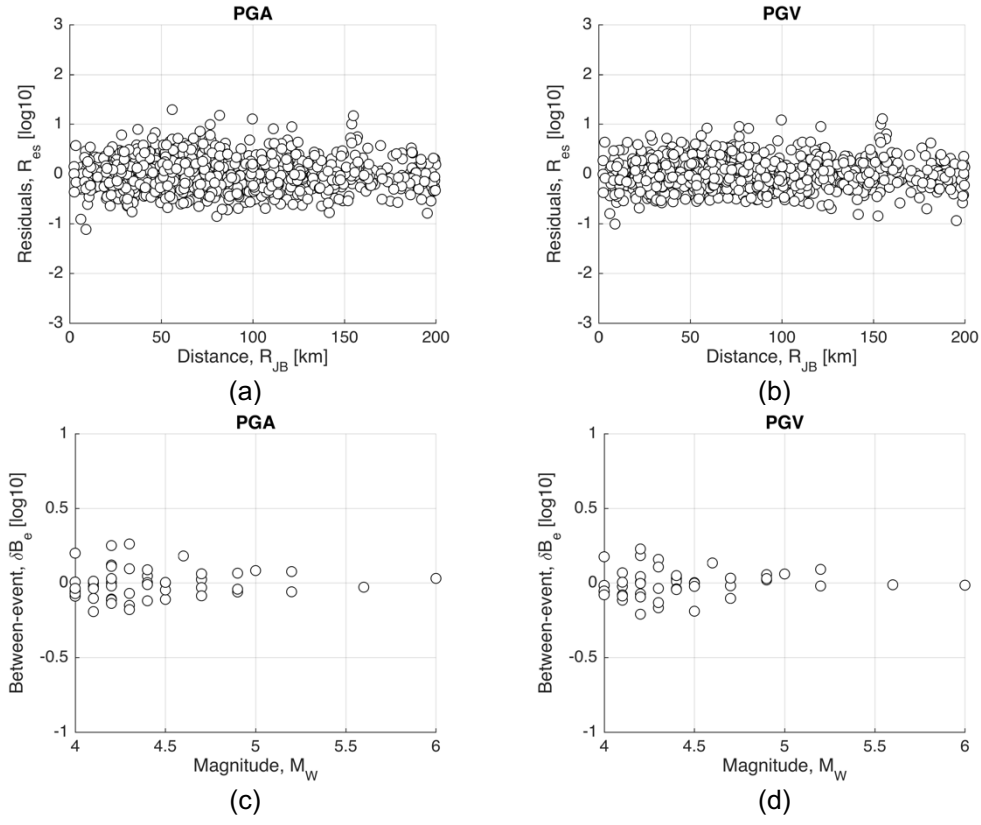

Figure 6. *Residuals of SI17ref: a) PGA total residuals as a function of distance; b) PGV total residuals as a function of distance; c) PGA between-event residuals as a function of magnitude; d) PGV between-event residuals as a function of magnitude.*

Total residuals variability seems to be independent on distance, with most of the values in the range [-1 1]. As expected, between-event variability is larger at lower magnitudes, related to higher stress-drop variability of small earthquakes (Oth et al. 2010).
The PGA median predictions of the SI17ref for soil classes RR and GR are plotted as a function of distance and are compared to ITA10 EC8-A in Figure 7. We also report the

empirical data points used for the regression and, as expected, the GMPEs are not well constrained in near fault conditions, since very few recordings are available at distance lower than 10km.

We can observe that the predictions of RR class are systematically lower than those obtained for GR class. The average reduction over all intensity measures is about 60% and it is even higher than that observed for Italy, of about 35% (Felicetta et al. 2018). The predictions of ITA10 for EC8-A are found to be similar to those obtained for GR sites.

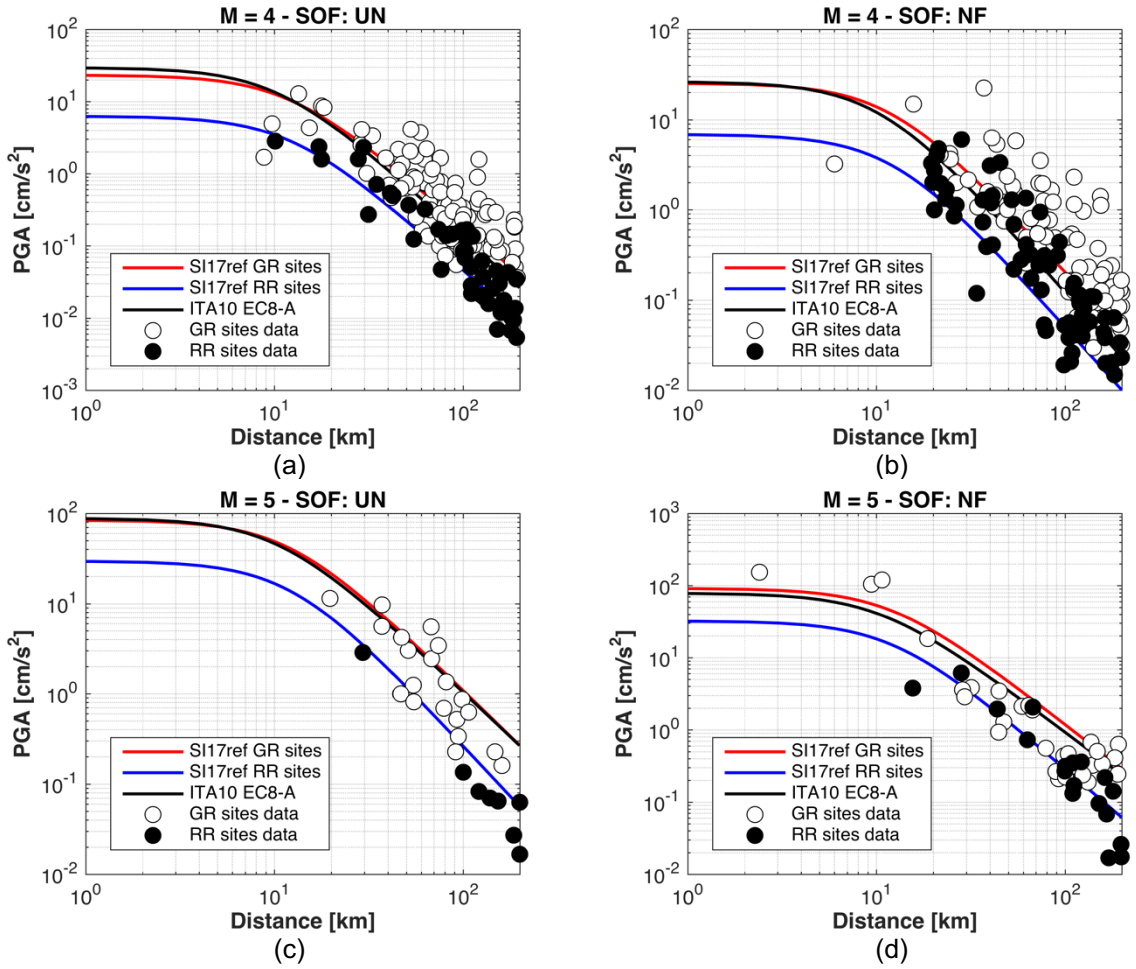

Figure 7. *SI17ref attenuation with distance: a) magnitude M=4.0, normal faulting (NF); a) magnitude M=4.0, undefined style of faulting (UN); a) magnitude M=5.0, normal faulting (NF); a) magnitude M=5.0, undefined style of faulting (UN). Black circles are the empirical data points of RR sites; white circles are the empirical data points of GR sites.*

Figure 8 shows the comparison between the standard deviations of SI17ref and ITA10 for the intensity measure considered in the GMPEs calibration. The total variabilities of the two models are similar, with a slight reduction of σ at longer periods of about 6%. The between-event standard deviation τ of SI17ref is significantly lower than ITA10, with a reduction in the range of 40-50%. This evidence is expected since a regional dataset is used for GMPEs calibration (see also Lanzano et al. 2016) and the event metadata in ESM were revised and improved with respect to those used for ITA10. As a result, the within-event variability of SI17ref is larger than ITA10.

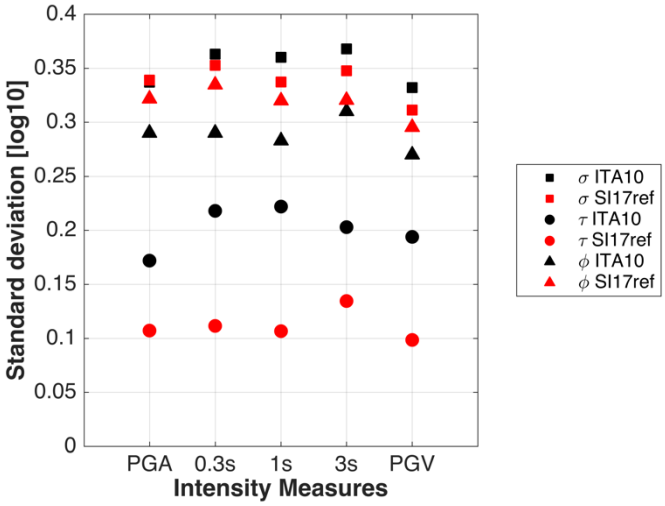

Figure 8. *Standard deviations of SI17ref and ITA10. σ, τ and ϕ are the standard deviations of the total, between-event and within-event residuals, respectively.*

Hybrid GMPEs

We preliminary compared the different datasets (empirical and simulated) we want to use to calibrate the hybrid ground motion model. The magnitude-distance distributions of the three datasets (EXSIM, SMSIM and recorded) are shown in Figure 9.

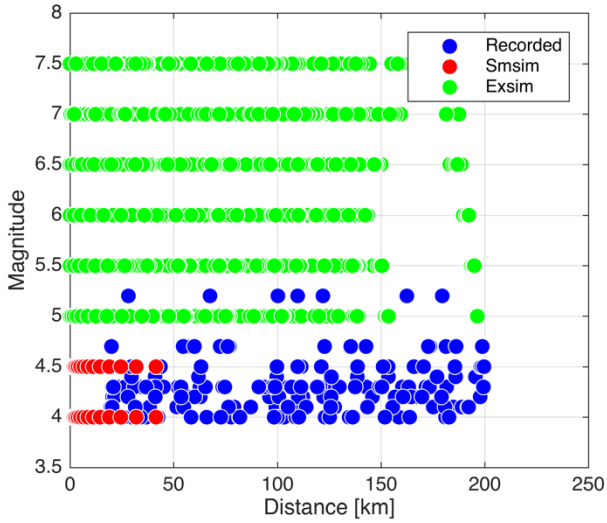

Figure 9. *Magnitude – distance distribution of the calibration dataset of the hybrid GMPEs.*

Since the simulations were performed for outcropping rock without topographic amplifications, we considered only recorded data relative to reference rock (RR) stations (blue circles), which corresponds to about 180 records. We decided to use the SMSIM data to constrain the near-fault ground motion at magnitudes 4.0 and 4.5 (red circles): for this reason, we decided to

include only records up to 50km, obtaining 3,648 usable records. No selection criteria are applied to EXSIM dataset, which encompasses more the 187,000 records (green circles). The empirical data are the 0.09% of the mixed dataset, while SMSIM and EXSIM datasets corresponds to 1.91% and 98%, respectively. This records imbalance makes impossible to obtain a hybrid GMPE from the combined data, because of the strong predominance of simulated data with respect to empirical ones.
In order to use a more balanced dataset, we assumed that all the empirical data corresponds to 15% of the calibration dataset, while percentage of SMSIM and EXSIM contribution was set to 20% and 65%, respectively. We randomly sampled the synthetic datasets, respecting the fixed proportions, obtaining a testing dataset composed by 1200 records (180 empirical, 240 SMSIM and 780 EXSIM).
The record distributions of a generic calibration dataset (named SET1) as a function of magnitude, distance and style of faulting are shown in Figure 10.

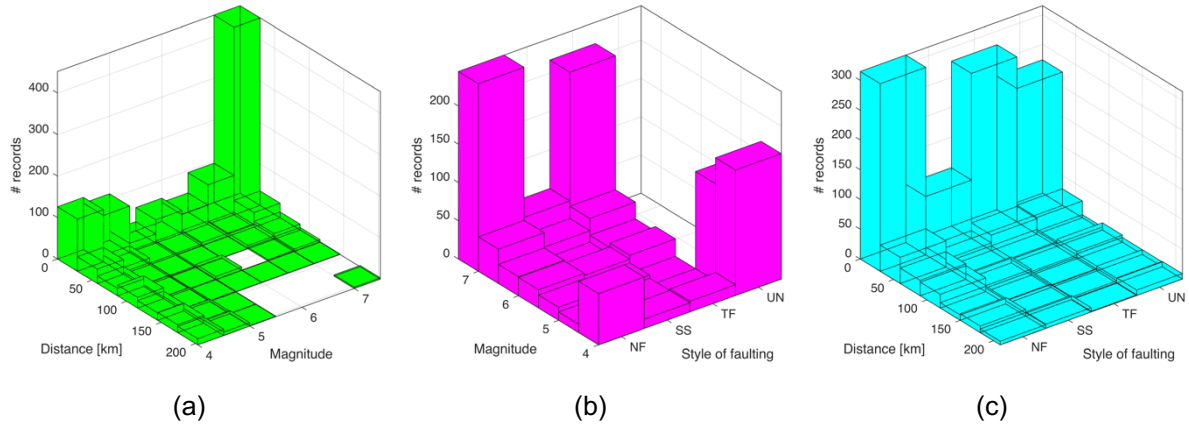

Figure 10. *Records histograms of a generic dataset (SET1) of the hybrid GMPEs calibration: a) magnitude vs. distance; b) magnitude vs. style of faulting; c) distance vs. style of faulting. NF: normal faulting; SS: strike-slip; TF: reverse faulting; UN: undefined.*

SET1 is still not completely balanced, since some distance-magnitude ranges are not covered by data, e.g. the distances higher than 150km and the magnitudes larger than 5.0. On the other side, SET1 has a consistent amount of data (more than 400) for the largest magnitudes (7.0 and 7.5) and distances lower than 50km.
Similarly, there is a lacking of data for undefined style of faulting (UN) and magnitude larger than 5.0. This evidence is related to the characteristics of the simulations: EXSIM data (M>5.0) are derived from finite fault simulations and the style of faulting is always known; SMSIM data are point-source simulations and no focal mechanisms is associated to the records (they are flagged as undefined).
Figure 11 reports the distribution of PGA and SA at 3s, as a function of distance for several classes of magnitudes. SET1 is able to reproduce the ground motion attenuation with distance and the scaling with magnitude. Moreover, especially at high frequencies, a magnitude-dependent attenuation is also noticeable.
We used the same functional form of Eq. [4.1], without the site effect term (F_S), since a model for reference rock (F_S=0) was only derived. Differently from empirical GMPEs, we also calibrated the model for reverse faulting. Despite the simulations are related to a set of

scenarios (D'Amico et al. 2018), we do not separate the residuals, since they can be poorly represented when we perform the random selection of the dataset.

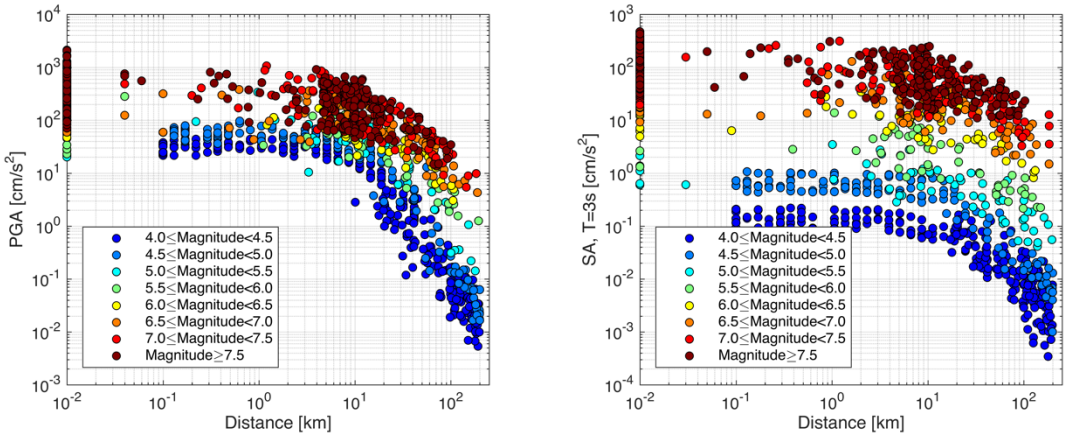

Figure 11. *Distribution of ground-motion parameters of SET1 as a function of distance for different classes of magnitudes: a) PGA; b) Spectral acceleration (SA) ordinates at T=3s.*

Since the coefficients are dependent on the random selection of the simulated data, we considered 50 different replications of the original dataset and estimated the median value and the variability of each calibration coefficient. Each replication had same number of records, respecting the proportions among the three different datasets. Table 4 show the median coefficients and the associated uncertainty of the hybrid GMPEs (named SI17hyb). The aleatory variability (σ) was estimated through the error propagation of the standard deviations of the residuals of the different replications.

Table 4. *Median values and standard deviations of the coefficients of SI17hyb.*

Coefficients		**Intensity Measures (IMs)**				
		PGA	**SA 0.3s**	**SA 1s**	**SA 3s**	**PGV**
a	*median*	3.713	4.031	3.446	2.665	2.477
	st. dev.	0.046	0.048	0.043	0.048	0.043
b_1	*median*	-0.384	-0.073	0.069	0.363	-0.03
	st. dev.	0.021	0.027	0.022	0.022	0.022
b_2	*median*	-0.056	-0.131	-0.155	-0.117	-0.054
	st. dev.	0.007	0.008	0.007	0.007	0.007
c_1	*median*	-2.242	-1.776	-1.519	-1.38	-1.859
	st. dev.	0.02	0.016	0.012	0.015	0.016
c_2	*median*	0.526	0.276	0.231	0.219	0.422
	st. dev.	0.013	0.015	0.014	0.014	0.014
h *[km]*	*median*	10.33	11.42	10.5	10.23	10.17
	st. dev.	0.173	0.13	0.137	0.149	0.18
f_{NF}	*median*	0.052	0.065	0.082	0.098	0.073
	st. dev.	0.014	0.014	0.012	0.015	0.014
f_{SS}	*median*	0.105	0.098	0.066	0.055	0.077
	st. dev.	0.02	0.021	0.015	0.017	0.018

f_{TF}	*median*	-0.056	-0.055	-0.048	-0.052	-0.054
	st. dev.	0.016	0.017	0.013	0.013	0.014
σ		0.299	0.289	0.278	0.271	0.265

The uncertainties of the calibration coefficients are significantly lower with respect to those calculated by Bindi et al. (2011) for ITA10, which considered 40 bootstrap replications of the starting dataset.
Figure 12a shows the PGA total residuals of SI17hyb, as a function of distance, with respect to the SET1 replication of the dataset (see Figures 10 and 11). Figures 12b and 12c plot the SI17hyb PGA residuals of EXSIM and SMSIM datasets, respectively. Figures 12d, 12e and 12f report the same plots of 12a, 12b and 12c for PGV.

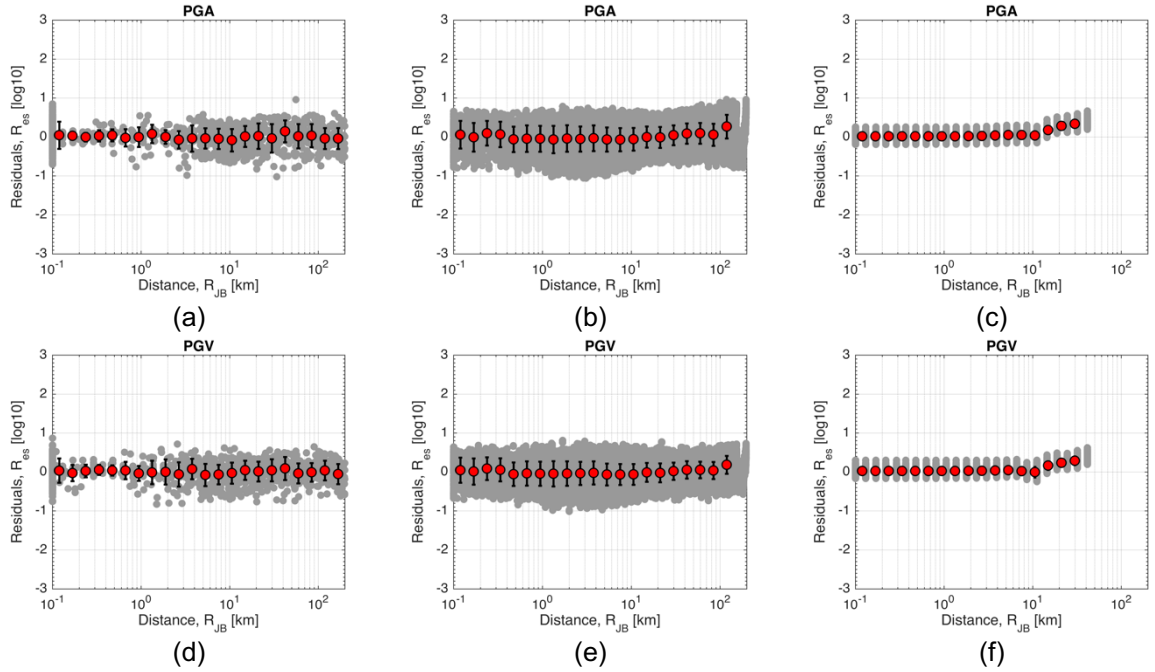

Figure 12. *Total residuals of SI17hyb as a function of distance: a) PGA residuals of SET1; b) PGA residuals of EXSIM dataset; c) PGA residuals of SMSIM dataset; d) PGV residuals of SET1; b) PGV residuals of EXSIM dataset; c) PGX residuals of SMSIM dataset.*

No trends with distance is observed for the residual plots of the generic SET1 replication; EXSIM residuals are unbiased, except for distances larger than 100km, where slight positive residuals are observed; SMSIM residuals exhibits a positive trend after 10 km, because these data were not used for GMPEs calibration.

The PGA median predictions (± standard deviations) of the SI17hyb (black curves) and SI17ref (grey curves) and the data point of the original dataset (Figure 9) are plotted as a function of distance in Figure 13 for different magnitudes and focal mechanisms. SI17ref predictions reported in Figure 13e and 13f are calculated outside of the validity range of the GMPEs, since they are calibrated up to 6.0.
The SI17hyb predictions are significantly different from SI17ref in near-fault conditions, since the hybrid GMPEs are better constrained by simulated data, showing larger median values.

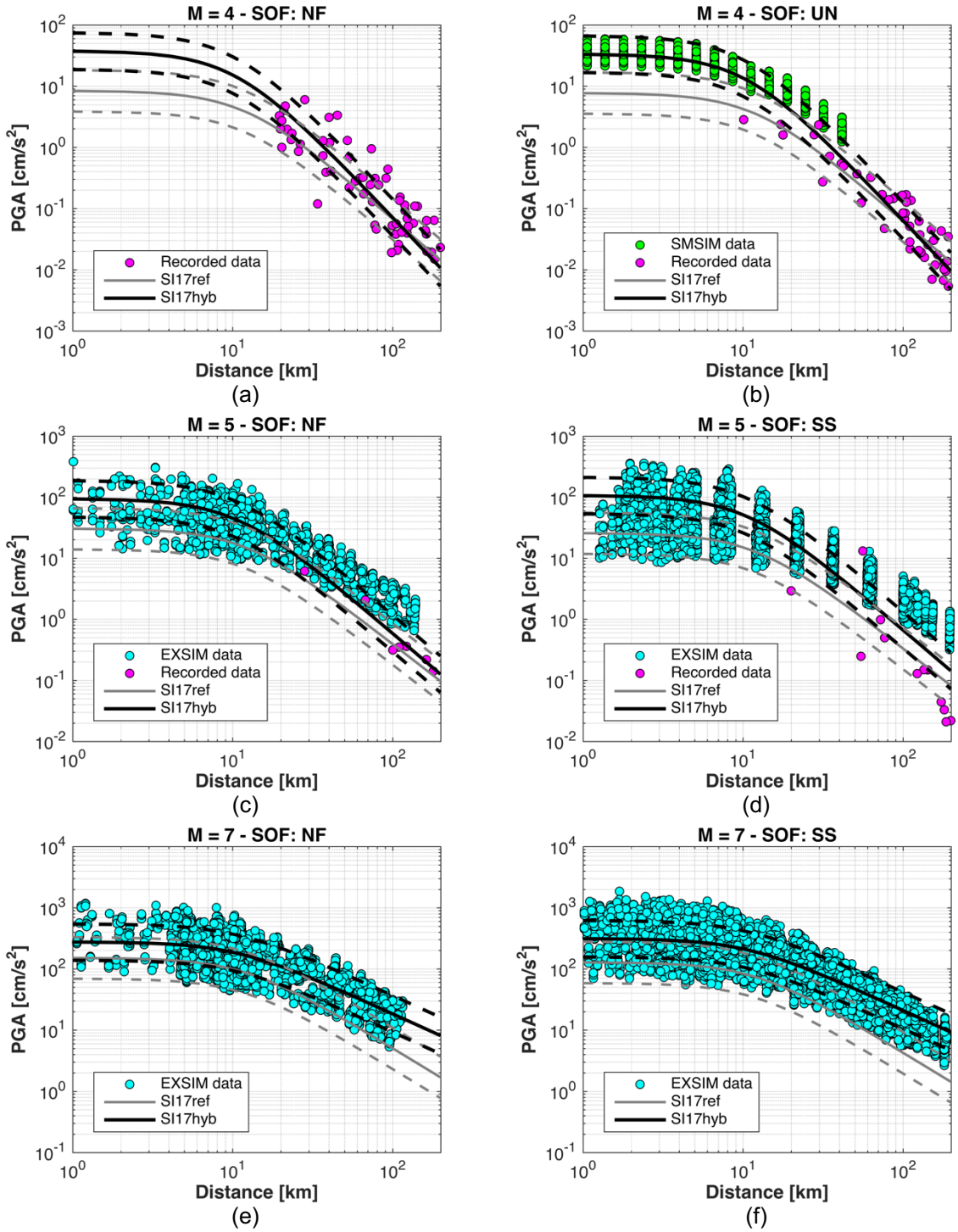

Figure 13. *PGA attenuation of hybrid (SI17hyb) and empirical (SI17ref) GMPEs with distance: a) magnitude M=4.0, normal faulting (NF); b) magnitude M=4.0, undefined style of faulting (UN); c) magnitude M=5.0, normal faulting (NF); d) magnitude M=5.0, strike-slip (SS); e) magnitude M=7.0, normal faulting (NF); f) magnitude M=7.0, strike-slip (SS). Magenta circles are the empirical data points; green circles are the SMSIM data points; cyan circles are the EXSIM data points.*

Table 5 reports the percentage increments of predictions of SI17hyb with respect to SI17ref, in near fault conditions (R=0.1km), for different magnitudes. The results are averaged over the predictions for the different style of faulting (normal, strike-slip and undefined focal mechanisms).

Table 5. *Percentage increments of prediction values of SI17hyb with respect to SI17ref ($Y_{SI17hyb}$- $Y_{SI17ref}$/ $Y_{SI17ref}$) at R=0,1km.*

Percentage increment [%]	M=4.0	M=5.0	M=6.0	M=7.0
PGA	394.0	242.3	153.6	100.8
SA T=0.3s	25.6	77.5	63.6	13.1
SA T=1s	65.2	64.9	42.1	9.8
SA T=3s	13.0	48.7	69.4	66.4
PGV	188.2	151.3	104.9	56.2

Significant increments of predictions are found for PGA and lower magnitudes, with a maximum value (394%) which approximately corresponds to a factor of 5.
At longer distances, the predictions of hybrid GMPEs are more influenced by empirical data, since they attenuate faster with distances, with respect to simulated data. Therefore, for the simulation, we used functions from literature, and they can differ from distance scaling, observed from the empirical data.

Figure 14 compares the total variabilities of SI17hyb, SI17ref and ITA10. The total variabilities of the hybrid model are significantly lower than those obtained for the empirical GMPEs, with a reduction of about 17-20%. This result is related to the fact that the point-source (SMSIM) simulations are not able to reproduce the variability of a real dataset (Pacor et al. 2017).

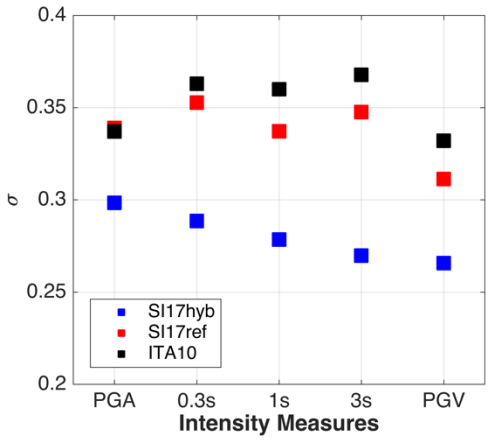

Figure 14. *Total standard deviation (σ) of the hybrid (SI17hyb) and empirical (SI17ref) GMPEs for Southern Italy. ITA10 (Bindi et al. 2011) is the reference model for Italy.*

Heteroscedastic model for aleatory uncertainty of hybrid GMPEs

The standard deviation of GMPEs measures the spreading of data around the median and represents the aleatory uncertainty associated to the predictions. In the last decade, a growing attention has been paid to the assessment of σ, due to its significant impact on PSHA for the design of critical infrastructures at long returning periods (Strasser et al. 2009; Ktenidou et al. 2017).

In most GMPEs, like for the hybrid model discussed in the previous section, the aleatory variability is assumed to be homoscedastic, i.e., independent of the variables included in the equation (Strasser et al. 2009). Several authors have found trends relating the sigma to one or more explanatory variables and therefore suggested heteroscedastic models, in which σ depends on the predictor variables. Most commonly, heteroscedastic models have found a decrease of the scatter with increasing magnitude (e.g. Sadigh et al., 1997; Ambraseys et al., 2005; Bommer et al., 2007). NGA-west introduced heteroscedastic aleatory variability in the prediction model, which are basically dependent on magnitude and other explanatory variables, such as non-linear site effects in soft sites (Abrahamson et al. 2014; Boore et al. 2014; Campbell and Bozorgnia 2014; Chiou and Youngs 2014).

In this section, we explore the possibility to build up a heteroscedastic model for the hybrid GMPEs SI17hyb, discussed in the previous section. Figure 13a reports the histogram of the SI17hyb generic calibration SET1 (same subset showed in Figure 9) as a function of magnitude. As observed before, the number of records for each magnitude bins varies from 40 to about 400 samples.

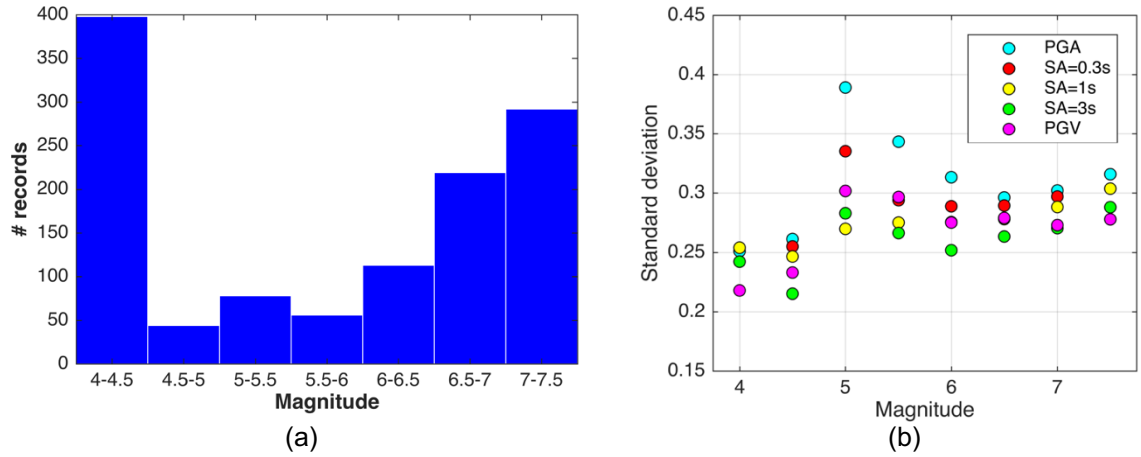

Figure 13. *a) Histogram of SET1 as a function of magnitude; b) Standard deviations of SI17hyb as function of magnitude bins.*

Figure 13b reports the total standard deviations as a function of magnitudes bins for the intensity measures of SI17hyb. The values of sigma significantly change with magnitude, showing lowest sigmas at magnitudes 4.0 and 4.5. This evidence is opposite to what is observed from empirical datasets, like, for example, for SI17ref in Figure 6c and 6d. It suggests that variabilities at low magnitudes, which is dominated by the SMSIM data, are not representative of a real variability. The larger magnitude is generally observed at M=5.0, decreasing for larger magnitudes: this behavior is instead similar to those observed from

recorded data (see NGA-West2 GMPEs). In the end, we decided to adopt the following model to describe the aleatory variability, σ:

$$\sigma(M) = \begin{cases} \sigma_1 & M \leq M_1 \\ \sigma_1 + \frac{\sigma_2 - \sigma_1}{2}(M - M_1) & M_1 \leq M \leq M_2 \\ \sigma_2 & M \geq M_2 \end{cases} \quad [5]$$

After some trial tests, we set the corner magnitudes to M_1=5.0 and M_2 = 6.0. We disregarded the values of sigma at 4.0 and 4.5 and attributed to σ_1 those calculated at M=5.0. σ_2 is calculated as an average value in the magnitude interval [6 7.5]. Table 6 gives the values of σ_1 and σ_2 of Eq. [5] for the IMs of SI17hyb.

Figure 14 represents the heteroscedastic model proposed to describe the aleatory variability of SI17hyb for the analyzed IMs. We add for comparison the models proposed by NGA-West2 and homoscedastic (independent on magnitude) value of sigma for SI17hyb.
Heteroscedastic sigma is significantly different from magnitude-independent model for PGA (Figure 14a), PGV (Figure 14e) and spectral ordinates at T=0.3s (Figure 14b). The model of Eq. [5] is in the range of that proposed for empirical models in literature for PGV and SA-T=0.3s. The PGA model exhibits values higher than the others, up to about 0.4 for M ≤ 5.0.
Standard deviation for the GMPEs in acceleration spectral ordinates at 1 and 3s are almost independent on magnitudes; hence, the simple homoscedastic model for aleatory variability can be used. The values are lower than those obtained from literature models, which also show a weaker dependence on M.

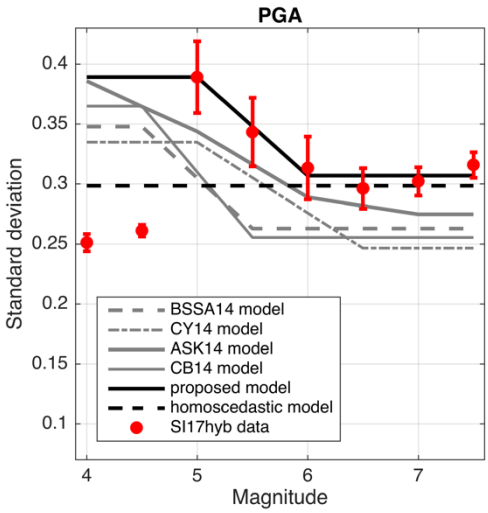

(a)

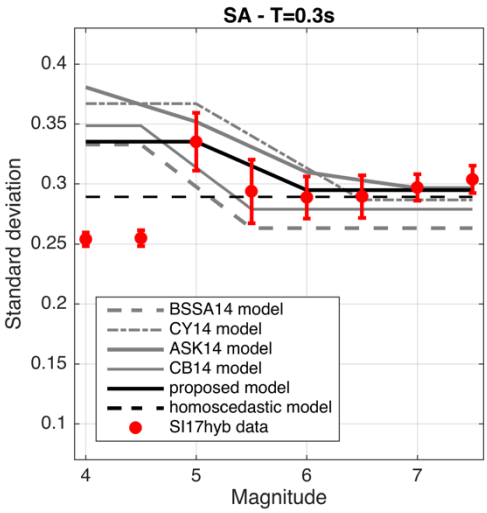

(b)

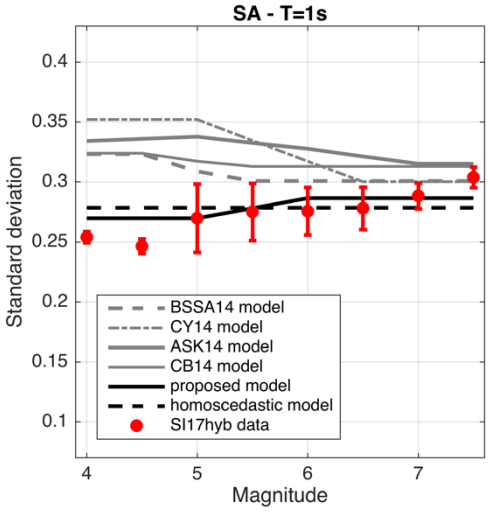

(c)

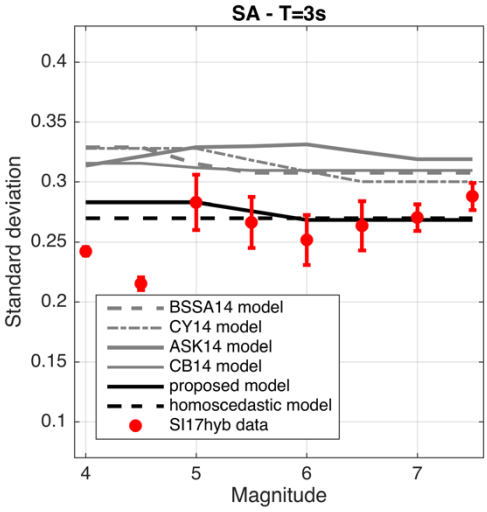

(d)

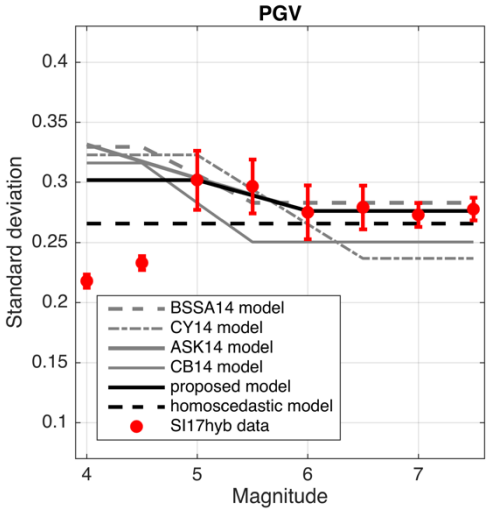

(e)

Table 6. *Coefficients of the SI17hyb heteroscedastic model of Eq. [5].*

Model coefficients	σ_1	σ_2
PGA	0.389	0.307
SA T=0.3s	0.335	0.295
SA T=1s	0.270	0.286
SA T=3s	0.283	0.268
PGV	0.302	0.276

Figure 14. *Heteroscedastic models of variability for SI17hyb: a) PGA; b) SA T=0.3s; c) SA T=1s; d) SA T=3s; e) PGV. ASK14: Abrahamson et al. (2014); BSSA14: Boore et al. (2014); CB14: Campbell and Bozorgnia (2014); CY14: Chiou and Youngs (2014).*

Conclusions and future developments

The objective of the HYPSTHER project is to develop a methodological approach to retrieve ground motion prediction models, integrating recorded and synthetic data. The results discussed in this deliverable represent the core of the research project.

The study area is characterized by high hazard levels and by the lack of empirical data needed to fully capture the peculiarities of the ground motion. With the few available empirical data (Puglia et al. 2018), especially at higher magnitudes (M>5.0) and in near fault conditions, we ranked a set of existing GMPEs, to be applied for shallow active crustal regions in Southern Italy. Once the best GMPEs is detected form from literature (i.e. that proposed by Bindi et al. 2011), we modified its functional form to tailor a ground motion model on the empirical data. As a result, we provided a set of GMPEs (named ***SI17ref***) for the geometric mean of the horizontal components of PGA, PGV and three ordinates of the acceleration response spectrum (T=0.3, 1 and 3s). We also exploited the results of Task 1 (Puglia et al. 2018) to predict the ground motion at reference rock, i.e. sites of outcropping rock without amplifications in the frequency range of engineering interest. The predictions of reference rock sites are significantly lower than those predicted for Italian rock sites by Bindi et al. (2011), of about 60%. The ***SI17ref*** sigma is instead slightly reduced (on average 6%) with respect to Italian GMPEs.

Hybrid GMPEs are retrieved by the creation of a dataset combining the empirical data, the data simulated by EXSIM and SMSIM, provided by Task 2 (D'Amico et al. 2018). Since the empirical dataset represents only the 0.1% of the simulated data, we randomly sampled the synthetic datasets, creating a set of 50 calibration datasets, each composed by 1200 records. The coefficients of the hybrid GMPEs (named ***SI17hyb***) are estimated as the median value of the calibration coefficients of the 50 replications. The standard deviations were estimated through the error propagation of the variabilities of each replicated GMPEs.
The use of hybrid ground-motion dataset is efficient since:

- ***SI17hyb*** predictions are larger with respect to ***SI17ref*** in near-fault conditions for PGA and lower magnitudes, with a maximum increasing value which corresponds to a factor of 5;
- ***SI17hyb*** predictions at distances larger than 50km are controlled by empirical data, because they attenuate faster with distances, with respect to simulated data;
- ***SI17hyb*** aleatory variability (σ) is significantly lower than those obtained for the empirical GMPEs (***SI17ref***), with an average reduction of about 17-20%.

Since the assessment of σ is critical for PSHA at long returning periods, we decided to build up a magnitude-dependent model for aleatory variability, similar to those proposed in the framework of NGA-West2. We decided to not take into account the variabilities at low magnitudes (M<5), since they are dominated by the SMSIM data, which are very low and not representative of an empirical dataset. The proposed models differ from magnitude independent sigma for PGA, PGV and spectral ordinates at T=0.3s. Homoscedastic models for acceleration spectral ordinates at long periods (1 and 3s) can be used, since standard deviations are almost independent on magnitudes.

The future developments of this work include:

- A strategy to randomly sample the synthetic datasets in order to have a homogeneous distribution of data in magnitude-distance space;
- The introduction of the components of the residuals, through the random effect model, to build up a non-ergodic hybrid GMPEs;
- The introduction of other explanatory variables in the functional form, like the stress parameters, which strongly influenced the waveform amplitudes.

The empirical (***SI17ref***) and hybrid (***SI17hyb***) prediction models have been used in Task 4 for hazard calculation (Santulin et al. 2018), to assess the impact on the design of critical infrastructures. In this way, the hybrid models could be tested to be used in a next generation of the MPS (Italian acronym for National Seismic Hazard Maps).

Electronic supplements

Electronic supplements include the tables of the coefficients of SI17ref and SI17hyb and are downloadable from HYPSTER website (http://hypsther.mi.ingv.it).

References

Abrahamson NA, Youngs RR (1992). A stable algorithm for regression analyses using the random effects model. Bulletin of the Seismological Society of America, 82(1), 505-510.

Abrahamson NA, Silva WJ, Kamai R (2014). Summary of the ASK14 ground motion relation for active crustal regions. Earthquake Spectra, 30(3), 1025-1055.

Akkar S, Bommer JJ (2010). Empirical equations for the prediction of PGA, PGV, and spectral accelerations in Europe, the Mediterranean region, and the Middle East. Seismological Research Letters, 81(2), 195-206.

Akkar S, Sandıkkaya MA, Şenyurt M, Sisi AA, Ay BÖ, Traversa P, Douglas J, Cotton F, Luzi L, Hernandez B, Godey S (2014a). Reference database for seismic ground-motion in Europe (RESORCE). Bulletin of Earthquake Engineering, 12 (1), 311-339.

Akkar S, Sandıkkaya MA, Bommer JJ (2014b). Empirical ground-motion models for point- and extended-source crustal earthquake scenarios in Europe and the Middle East, Bulletin of Earthquake Engineering, 12(1), 359–387, doi:10.1007/s10518-013-9461-4.

Al-Atik L, Abrahamson N, Bommer JJ, Scherbaum F, Cotton F, Kuehn N (2010). The variability of ground-motion prediction models and its components. Seismological Research Letters, 81(5), 794-801.

Ambraseys NN, Douglas J, Sarma SK, Smit PM (2005). Equations for the estimation of strong ground motions from shal- low crustal earthquakes using data from Europe and the Middle East: Horizontal peak ground acceleration and spectral acceleration. Bulletin of Earthquake Engineering 3 (1), 1–53.

Ancheta TD, Darragh RB, Stewart JP, Seyhan E, Silva WJ, Chiou BS-J, Wooddell KE, Graves RW, Kottke AR, Boore DM, Kishida T, Donahue JL (2014). NGA-West2 database. Earthquake Spectra, 30(3), 989-1005.

Atkinson GM (2008). Ground motion prediction equations for eastern North America from a referenced empirical approach: Implications for epistemic uncertainty, Bull. Seismol. Soc. Am. 98, 1304–1318.

Bindi D, Pacor F, Luzi L, Puglia R, Massa M, Ameri G, Paolucci R (2011): Ground motion prediction equations derived from the Italian strong motion database. Bulletin of Earthquake Engineering, 9 (6), 1899-1920.

Bindi D, Massa M, Luzi L, Ameri G, Pacor F, Puglia R, Augliera P (2014), Pan-European ground-motion prediction equations for the average horizontal component of PGA, PGV, and 5 %-damped PSA at spectral periods up to 3.0 s using the RESORCE dataset, Bulletin of Earthquake Engineering, 12(1), 391–430, doi:10.1007/s10518-013-9525-5.

Bommer JJ, Stafford PJ, Alarcón JE, Akkar S (2007). The influence of magnitude range on empirical ground-motion prediction. Bulletin of the Seismological Society of America 97 (6), 2,152–2,170.

Bommer JJ, Douglas J, Scherbaum F, Cotton F, Bungum H, Fah D (2010), On the Selection of Ground-Motion Prediction Equations for Seismic Hazard Analysis, Seismological Research Letters, 81(5), 783–793, doi:10.1785/gssrl.81.5.783.

Boore DM, Stewart JP, Seyhan E, Atkinson GM (2014). NGA-West2 equations for predicting PGA, PGV, and 5% damped PSA for shallow crustal earthquakes. Earthquake Spectra, 30(3), 1057-1085.

Bozorgnia Y, Abrahamson NA, Al-Atik L, Ancheta TD, Atkinson GM, Baker JW, Baltay A, Boore DM, Campbell KW, Chiou BS-J, Darragh R, Day S, Donahue J, Graves RW, Gregor N, Hanks T, Idriss IM, Kamai R, Kishida T, Kottke A, Mahin SA, Rezaeian S, Rowshandel B, Seyan E, Shahi S, Shantz T, Silva W, Spudich P, Stewart JP, Watson-Lamprey J, Wooddell K, Youngs R (2014). NGA-West2 research project. Earthquake Spectra, 30(3), 973-987.

Campbell KW (2003). Prediction of strong ground motion using the hybrid empirical method and its use in the development of ground- motion (attenuation) relations in eastern North America, Bulletin of the Seismological Society of America, 93, 1012–1033.

Campbell KW, Bozorgnia Y (2014). NGA-West2 ground motion model for the average horizontal components of PGA, PGV, and 5% damped linear acceleration response spectra. Earthquake Spectra, 30(3), 1087-1115.

Cauzzi C, Faccioli E, Vanini M, Bianchini A (2015), Updated predictive equations for broad-band (0.01–10 s) horizontal response spectra and peak ground motions, based on a global dataset of digital acceleration records, Bulletin of Earthquake Engineering, doi:10.1007/s10518-014-9685-y.

CEN (2004): Design of structures for earthquake resistance, Part 1: General rules, seismic actions and rules for buildings, EN 1998-1, European Committee for Standardization (CEN), Brussels, http://www.cen.eu/cenorm/homepage.htm.

Chiou BSJ, Youngs RR (2014). Update of the Chiou and Youngs NGA model for the average horizontal component of peak ground motion and response spectra. Earthquake Spectra, 30(3), 1117-1153.

Cotton F, Scherbaum F, Bommer JJ, Bungum H (2006), Criteria for Selecting and Adjusting Ground-Motion Models for Specific Target Regions: Application to Central Europe and Rock Sites, J Seismol, 10(2), 137–156, doi:10.1007/s10950-005-9006-7.

D'Amico M, Tiberti MM, Russo E, Gomez-Capera AA (2018). Ground motion simulation. Istituto Nazionale di Geofisica e Vulcanologia, HYPSTHER project, http://hypsther.mi.ingv.it/ - doi: 10.5281/zenodo.1162203.

Dalguer L, Askan A, Goo Song S (2014). Near fault ground motion. Report Task 13.7 NERA EU Project.

Delavaud E, Cotton F, Akkar S, Scherbaum F, Danciu L, Beauval C, Drouet S, Douglas J, Basili R, Sandikkaya MA, Segou M, Faccioli E, Theodoulidis N (2011), Toward a ground-motion logic tree for probabilistic seismic hazard assessment in Europe, Journal of Seismology, 16(3), 451–473, doi:10.1007/s10950-012-9281-z.

Douglas J, Akkar S, Ameri G, Bard PY, Bindi D, Bommer JJ, Bora SS, Cotton F, Derras B, Hermkes M, Kuehn NM, Luzi L, Massa M, Pacor F, Riggelsen C, Sandıkkaya MA, Scherbaum F, Stafford PJ, Traversa P (2014): Comparisons among the five ground-motion models developed using RESORCE for the prediction of response spectral accelerations due to earthquakes in Europe and the Middle East. Bulletin of Earthquake Engineering, 12 (1), 341-358.

Felicetta C, Lanzano G, D'Amico M, Puglia R, Luzi L, Pacor F (2018). Ground motion model for reference rock sites in Italy. Soil Dynamics and Earthquake Engineering, DOI: 10.1016/j.soildyn.2018.01.024.

Goulet CA, Abrahamson N, Bozorgnia Y (2011): NGA-East final project plan. Report. Pacific Earthquake Engineering Research Center (PEER).

Ktenidou OJ, Roumelioti Z, Abrahamson N, Cotton F, Pitilakis K, Hollender F (2017) Understanding single-station ground motion variability and uncertainty (sigma): lessons learnt from EUROSEISTEST. Bull Earthq Eng. doi:10.1007/s10518-017-0098-6.

Lanzano G, D'Amico M, Felicetta C, Puglia R, Luzi L, Pacor F, Bindi D (2016): Ground Motion Prediction Equations for region-specific PSHA. Bulletin of the Seismological Society of America, 106 (1), 73-92.

Michelini A., Luzi L., Lanzano G., Puglia R., Felicetta C., D'Amico M., Russo E., Pacor F., Faenza L., Lauciani V., Cultrera G., Milana G. (2017). Il terremoto di Casamicciola del 21 agosto 2017: osservazioni sul moto del suolo. https://ingvterremoti.wordpress.com (in Italian).

Oth A, Bindi D, Parolai S, Di Giacomo D (2010) Earthquake scaling characteristics and the scale-(in)de-pendence of seismic energy-to-moment ratio: insights from KiK-net data in Japan. Geophys Res Lett 37:L19304. doi:10.1029/2010GL044572

Pacor F, Ameri G, Gallovic F, D'Amico M (2017). Ground Motion variability from finite fault simulations. Proceedings of the 16th World Conference on Earthquake, 16WCEE, Santiago Chile, January 9th to 13th. Paper N° 2062.

Puglia R, Felicetta C, Russo E, Lanzano G (2018). Empirical flat-file generation. Istituto Nazionale di Geofisica e Vulcanologia, HYPSTHER project, http://hypsther.mi.ingv.it/ doi:10.5281/zenodo.1157975

Sadigh K, Chang C-Y, Egan JA, Makdisi F, Youngs RR (1997). Attenuation relationships for shallow crustal earthquakes based on California strong motion data. Seismological Research Letters 68 (1), 180–189.

Santulin M, D'Amico M, Lanzano G (2018). Hazard assessment. Istituto Nazionale di Geofisica e Vulcanologia, HYPSTHER project, http://hypsther.mi.ingv.it/.

Scherbaum, F, Delavaud E, Riggelsen C (2009). Model selection in seismic hazard analysis: An information–theoretic perspective, Bulletin of the Seismological Society of America, 99, no. 6, 3234–3247.

Strasser FO, Abrahamson NA, Bommer JJ (2009). Sigma: Issues, insights, and challenges. Seismological Research Letters, 80(1), 40-56.

Tusa G, Langer H (2016). Prediction of ground motion parameters for the volcanic area of Mount Etna. Journal of Seismology, 20(1), 1-42.

Appendix A

Table A1. List of records with large residuals, excluded from GMPEs calibration.

#	Net	Station	ID event	Event time	ML
1	IV	SN1	EMSC-20130324_0000133	2013-03-24	4.3
2	IV	SN1	IT-2013-0001	2013-01-04	4.4
3	IT	TES	IT-2012-0055	2012-04-13	4.3
4	IV	LADO	EMSC-20120528_0000003	2012-05-28	4.3
5	IV	LADO	EMSC-20140325_0000041	2014-03-25	3.6
6	IV	LADO	EMSC-20140604_0000074	2014-06-04	3.7
7	IV	LADO	EMSC-20140606_0000048	2014-06-06	3.9
8	IV	LADO	EMSC-20140731_0000006	2014-07-31	3.5
9	IV	LADO	EMSC-20141228_0000068	2014-12-28	4.4
10	IV	LADO	EMSC-20150803_0000020	2015-08-03	4.1
11	IV	LADO	IT-2010-0027	2010-06-16	4.1
12	IV	LADO	IT-2010-0047	2010-10-15	4.2
13	IV	LADO	IT-2011-0008	2011-03-25	3.5
14	IV	LADO	IT-2011-0009	2011-03-25	3.8
15	IV	LADO	IT-2011-0083	2011-09-19	3.6
16	IV	LADO	IT-2011-0088	2011-10-14	3.7
17	IV	LADO	IT-2012-0084	2012-09-14	3.7
18	IV	LADO	IT-2012-0086	2012-10-01	3.7
19	IT	GEA	EMSC-20160525_0000113	2016-05-25	4.0
20	IT	ISI	EMSC-20160525_0000113	2016-05-25	4.0
21	IT	LCA	EMSC-20160525_0000113	2016-05-25	4.0
22	IT	LNT	EMSC-20160525_0000113	2016-05-25	4.0
23	IT	PCH	EMSC-20160525_0000113	2016-05-25	4.0
24	IT	PLZ	EMSC-20160525_0000113	2016-05-25	4.0
25	IT	PPL1	EMSC-20160525_0000113	2016-05-25	4.0
26	IT	RCU	EMSC-20160525_0000113	2016-05-25	4.0
27	IT	RGS	EMSC-20160525_0000113	2016-05-25	4.0
28	IT	SRC	EMSC-20160525_0000113	2016-05-25	4.0
29	IT	TOR	EMSC-20160525_0000113	2016-05-25	4.0
30	IT	VZZ	EMSC-20160525_0000113	2016-05-25	4.0
31	IV	PLAC	EMSC-20160525_0000113	2016-05-25	4.0
32	MN	CEL	EMSC-20160525_0000113	2016-05-25	4.0
33	IT	NAS	IT-1978-0003	1978-04-15	4.1
34	IT	PTT1	IT-1978-0003	1978-04-15	4.1
35	IV	IFIL	IT-2011-0097	2011-11-15	4.1

IV: Italian National Seismic Network, Istituto Nazionale di Geofisica e Vulcanologia, Italy.

IT: Italian Strong Motion Network, Dipartimento della Protezione Civile, Italy.

MN: Mediterranean Very Broadband Seismographic Network, Istituto Nazionale di Geofisica e Vulcanologia, Italy.

Disclaimer

Any result included in the document is based on the available scientific knowledge and is devoted to qualified users. Every risk due to the improper use of data or the use of inaccurate information is assumed by the user.

Creative Commons

Citation

This Deliverable must be cited as follow: "**Lanzano G, D'Amico M, Felicetta C, Puglia R (2018). GMPEs calibration.** Istituto Nazionale di Geofisica e Vulcanologia, HYPSTHER project, http://hypsther.mi.ingv.it/ - doi: 10.5281/zenodo.1162735".